Texture effects on design of Mg biodegradable stents

Maurizio Vedani · Qiang Ge · Wei Wu · Lorenza Petrini

Introduction

Magnesium has a poor formability at room temperature owing to its hexagonal close packed (hcp) structure with extremely limited slip systems. At room temperature the activity of (0001) basal plane preferentially occurs while at higher temperatures, the prismatic and pyramidal slip systems are also activated, significantly improving the material formability [1]. It is also known that strong crystallographic texture can be developed during plastic processes due to rotation of grains, leading to alignment of basal planes parallel to the main material flow direction such as the extrusion or rolling direction [2, 3]. Wrought magnesium components are believed to have better mechanical properties than cast alloys. However, the existence of this specific texture, commonly results in strong tension-compression anisotropy in several wrought magnesium alloys [4, 5].

Biodegradable metallic stents are devices belonging to a newly emerging cardiovascular technology which has the potential to eliminate long-term patient health risks associated with conventional, permanent stents. Magnesium and its alloys are considered as the ideal candidate for their biocompatibility and low corrosion resistance. Since mechanical properties are significantly different from those of commonly used stainless steel and cobal-chromium alloys, design of the Mg-alloy structure has to be performed considering all the peculiar features of this material, to achieve service performance and reliability comparable to those of permanent stents. Biodegradable Magnesium stents are manufactured starting from small-size tubes fabricated by hot extrusion, followed by cold drawing, laser cutting of the net and electrochemical polishing of the surfaces [6]. When introduced into the vessel by a catheter, the stent is then

M. Vedani · Q. Ge (✉)
Dipartimento di Meccanica, Politecnico di Milano,
Via G. La Masa 1,
20156 Milan, Italy
e-mail: qiang.ge@mail.polimi.it

W. Wu · L. Petrini
Dipartimento di Ingegneria Strutturale, Politecnico di Milano,
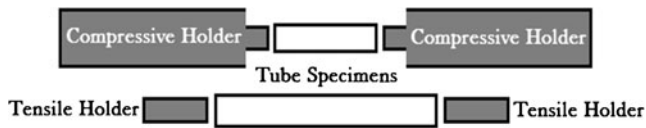Piazza Leonardo da Vinci 32,
20133 Milan, Italy

Fig. 1 Schematic of specimen holder for tension-compression test

expanded by an inflated balloon and the Mg alloy is subjected to significant plastic straining at body temperature. An early study also revealed that the recoil of the stent was the main reason for restenosis after 4 months from introduction into the vessel. Therefore, efforts to increase the radial strength of the stent have still to be done in order to improve patency rates of magnesium devices [7].

Finite element method was widely used to optimize the stent design [8–12]. However, up to now, detailed models accounting for the asymmetric tensile-compressive behavior of Mg were seldom considered. In this paper, the microstructure and crystallographic orientation developed during hot extrusion of the small tubes were investigated and the resulting mechanical compressive-tensile asymmetric properties were measured. Moreover, the relationship between material's texture condition and asymmetric property was discussed to improve the knowledge on biodegradable magnesium stent design.

Experimental procedures

The experimental materials used in this study were the ZM21 and AZ31B magnesium alloys. These materials were supplied in the form of commercially available wrought bars having a diameter of 15 mm. Hot-extrusion was carried out in the laboratory at die temperature of 410 °C and average strain rate of $2.78 \cdot 10^{-3} \, \mathrm{s}^{-1}$. A series of hollow tubes with outer diameter (D) ranging from 8 to 4 mm and inner diameter (d) from 6 to 3 mm were produced. The detailed experimental procedure for tube extrusion was reported in a previous work [13].

Texture evolution from the as received to the extruded materials was investigated by Electron Backscattering Diffraction (EBSD) technique. Specimens sectioned parallel to the extrusion direction were electro-polished by using a voltage of 1 to 5 V depending on sample size in a solution of 10 % nitric acid, 30 % glycerin and 60 % ethanol.

To assess material performance strictly related to microstructural conditions matching the stent precursors, the mechanical properties were measured both in tension and compression on samples directly cut from as extruded tubes to suitable gauge length. Tensile specimens had a gauge length of 30 mm for each extrusion diameter while compressive specimens had a reduced length of 20 mm to limit buckling phenomena during testing. A set of sample holders shown in Fig. 1 was used according to the different tube size to allow sample gripping during straining. The tube specimens were then treated as normal cylindrical samples and tested in a universal testing frame. A cross-head speed of 0.5 mm/min was chosen and a 10 mm gauge length extensometer was mounted on the central portion of the specimens. For both of compressive and tensile modes, data were collected up to strain of 2 % to avoid unwanted effects related to tube buckling in compression and sliding at grips in tension.

During processing (before and after hot extrusion) and after the tension-compression tests, microstructure was checked by optical and scanning electron microscopy to highlight possible modifications of microstructure induced by straining. A solution of 5 ml acetic acid and 6 g picric acid in 10 ml H_2O and 100 ml ethanol was used to reveal the metallographic grain structure.
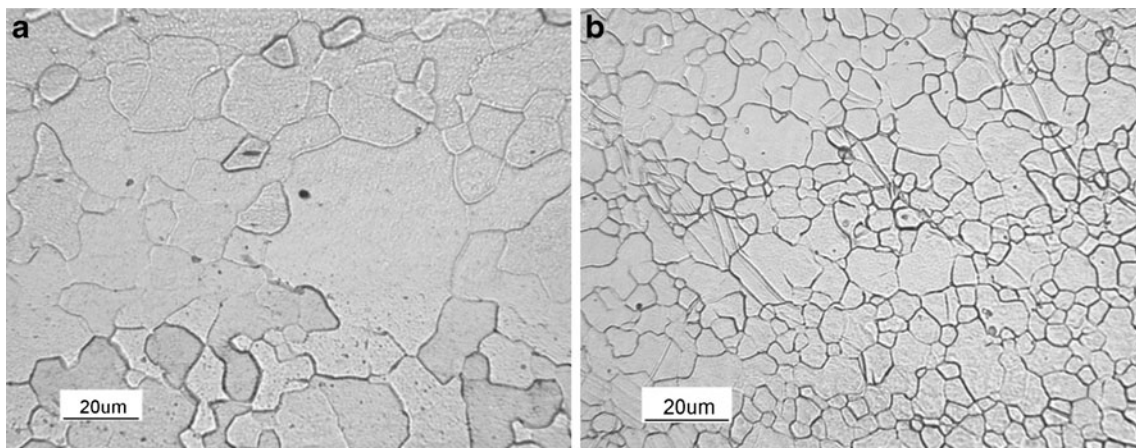

Fig. 2 Microstructure detected at mid-thickness of longitudinal sections of extruded D4d3 tubes. a Optical micrograph of ZM21 alloy; b optical micrograph of AZ31B alloy
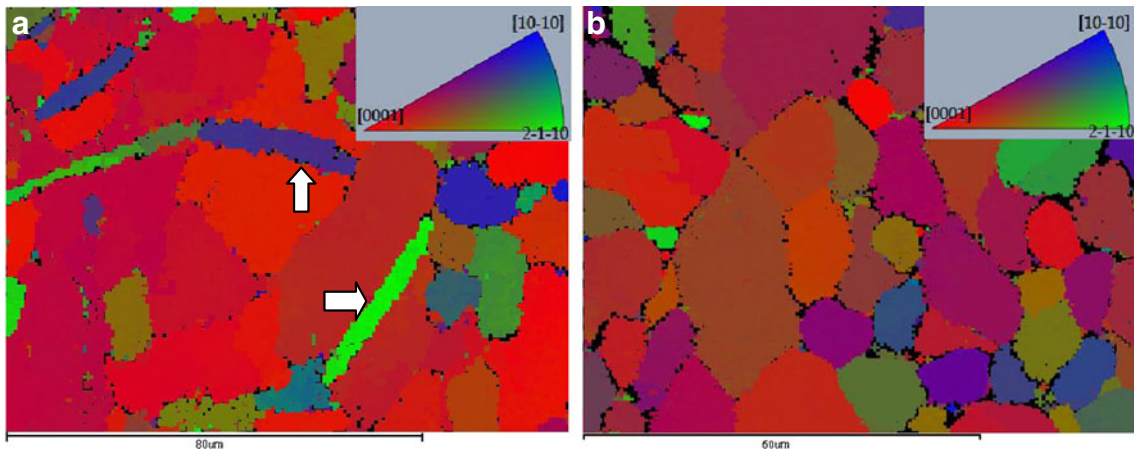
Fig. 3 Orientation map of extruded D4d3 tubes: **a** ZM21; **b** AZ31B

## Experimental results

Microstructure

In Fig. 2, the representative microstructure of extruded tubes D4d3 is shown. Hereafter, the size of the tubes will be stated by a capital D followed by the size of the outer diameter and a d followed by inner diameter, both in mm. The micrographs are taken from mid-thickness of longitudinal sections of ZM21 and AZ31B samples. For the ZM21 alloy, the concurrent action of temperature and strain during extrusion initially promoted recrystallization and then coarsening of a few sets of grains, as depicted in Fig. 2a. A relatively more refined microstructure with equiaxed grains was obtained by recrystallization and limited grain growth in the AZ31B alloy (Fig. 2b).

Crystallographic texture

The EBSD investigation was carried out along longitudinal sections of both the starting and the extruded alloys. The orientation maps gathered from EBSD analysis revealed a preferred orientation in both ZM21 and AZ31B extruded alloys as depicted in Fig. 3. The map clearly reveals that the predominant red grains feature their (0001) planes aligned parallel to the sample surface (longitudinal axial sections). Figure 3 also shows that twins can be recognized in the EBSD maps (see for instance the arrowed region in Fig. 3a). Texture and twinning were more developed in ZM21 alloy than in AZ31B alloy.

Figure 4 shows the inverse pole figures in a direction normal to longitudinal axis obtained from starting alloys. It is revealed that both of ZM21 and AZ31B starting alloys

Fig. 4 Inverse pole figures taken from longitudinal sections of the starting bars: **a** ZM21 and **b** AZ31B
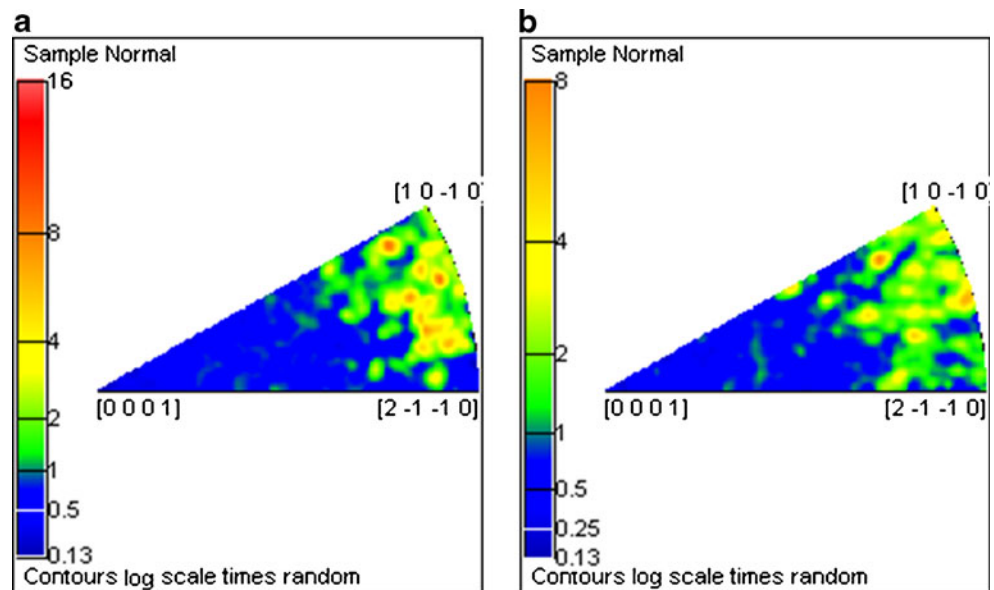
had a similar condition with a weak texture given by the prismatic planes {10–10} and {2-1-10} aligned along the longitudinal axis of the bars.

After the laboratory-scale extrusion, the texture of the small-size tubes clearly changed as depicted in Fig. 5. It is confirmed that both alloys, irrespective of tube size, show a typical (0001) extrusion texture, featuring the basal plane aligned parallel to the extrusion direction.

Mechanical properties

Figure 6 depicts the initial part of the tensile and compression stress-strain curves recorded for the ZM21 and AZ31B alloys. It is highlighted that yielding in compression occurs

at significantly lower stress than in tension. Values of the 0.2 % offset yield strength measured in tension and in compression are summarized in Table 1. As already stated, tests were performed on full-size cylindrical tube samples without machining a distinct gauge length due to small thickness limitations. Therefore, data about ultimate tensile strength and fracture elongation were not considered to be fully reliable and are not presented here.

It can be readily observed that both alloys feature a marked tension-compression asymmetry, the tensile yield strength being always significantly higher than that in compression. In ZM21 alloy, the yield stress in tension of the as received material is comparable to that found in the extruded tubes. However, a clear loss in strength is experienced in

Fig. 5 Inverse pole figures taken from longitudinal tube sections: a ZM21 D8d6 tube; b ZM21 D6d3 tube; c ZM21 D4d3 tube; d AZ31B D6d3 tube
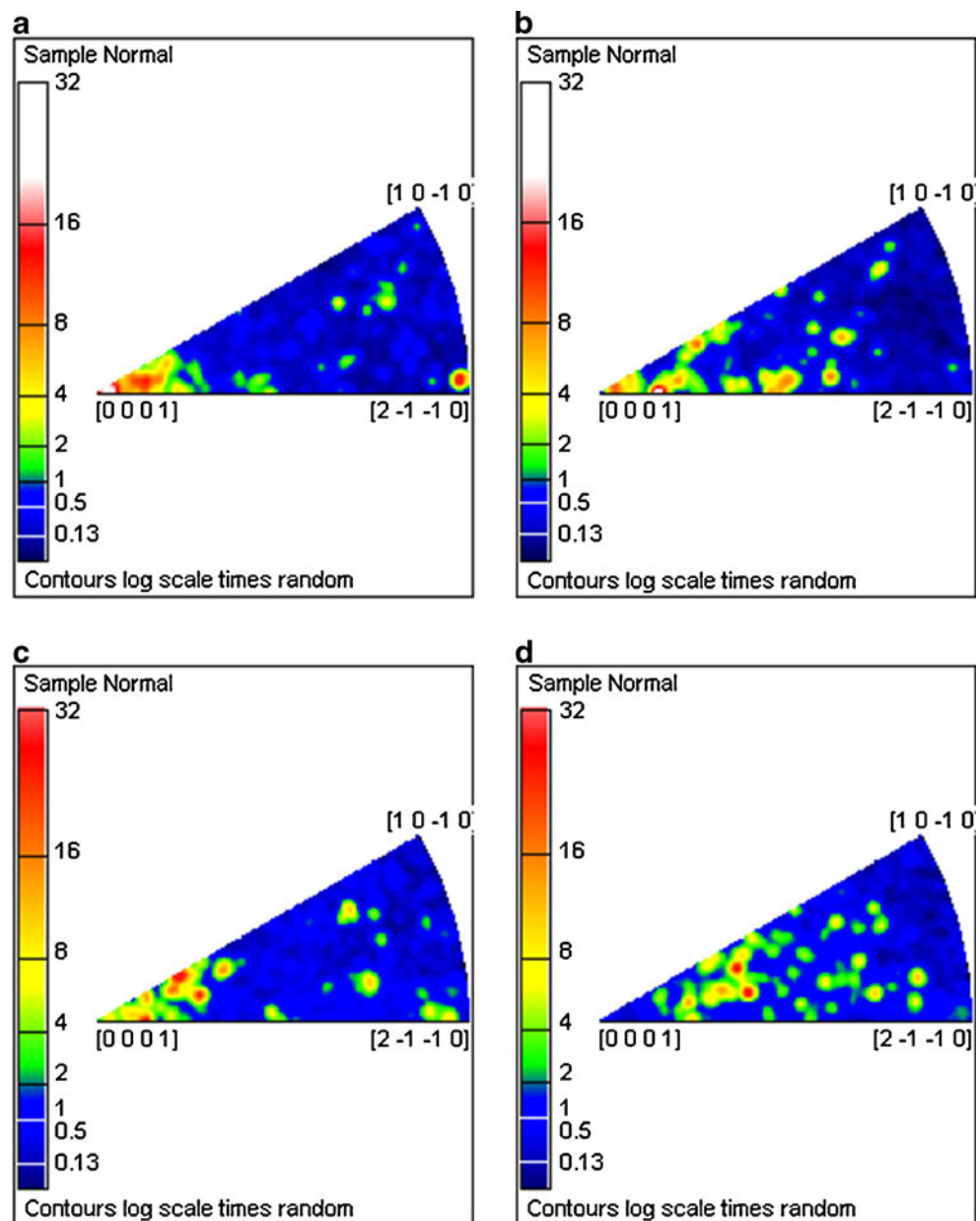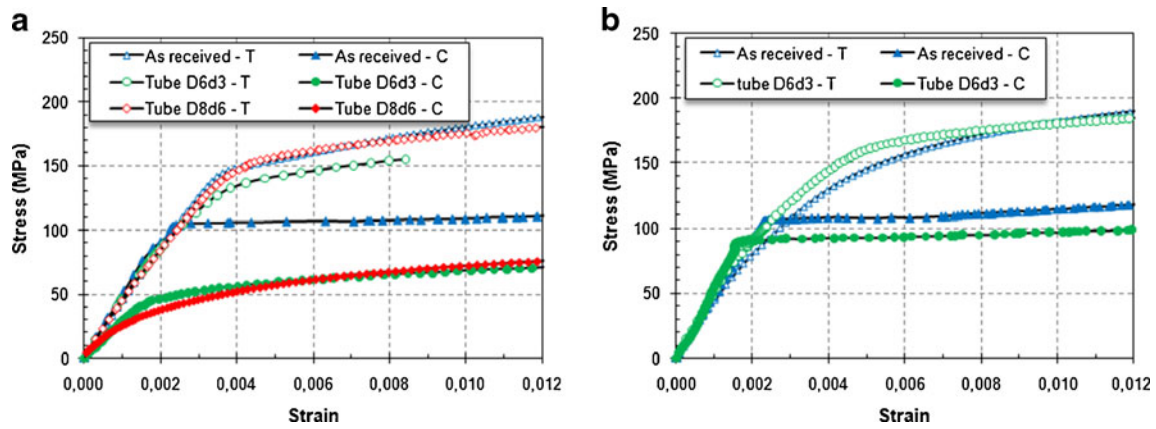
Fig. 6 Tensile and compression stress-strain curves detected on starting bars and on hot-extruded tubes. **a** ZM21 alloy; **b** AZ31B alloy

compression when moving from the as received bars to the extruded tubes. In the AZ31B alloy, extrusion led to a less evident drop in compressive strength, even though the above mentioned trend was still clearly visible.

Representative optical micrographs taken along the sectioned gauge length of the tension and compression strained specimens of the extruded ZM21 alloy are depicted in Fig. 7. A quite large amount of twins were detected in specimens subjected to compressive stress while very few twins were observed in the tensile strained specimens.

Discussion

Texture evolution during extrusion

Studies about hcp crystal structure of magnesium [14, 15] reported that the basal slip systems available at room temperature for plastic deformation do not satisfy the Taylor criterion requiring five independent easy slip systems for homogeneous and generalized ductility of polycrystalline metals. Other non basal slip systems such as the prismatic and pyramidal slip would offer six extra independent slip modes that could fulfill the requirement of plasticity and good workability. However, these non basal slip systems

become available only at high temperature in Mg and Mg alloys [16], suggesting that shaping of the tubes cannot be performed other than by hot extrusion. The starting wrought bars here investigated exhibited weak preferential orientation of (10–10) and (2-1-10) planes along longitudinal direction. On the contrary, a well developed basal texture was found in the AZ31B and ZM21 alloy tubes from laboratory scale extrusion at 410 °C.

Twinning and asymmetric mechanical behavior

In addition to dislocation slip, it was also reported that magnesium exhibits a strong propensity for mechanical twinning. Indeed, it is well known that twinning deformation modes play an important role during the deformation of hexagonal metals [17]. Despite the limited contribution of twinning itself to the total plasticity, the abrupt change of orientation due to twinning may give rise to the activation of other slip systems. The {10–12} <10–11> twin system is often observed in magnesium alloys and considered to be the preferential twinning system [18]. This kind of twinning preferably occurs when shear results from compressive stress applied parallel to the basal plane or from tensile stress applied perpendicularly to the same plane [19]. By the texture condition detected in the present extruded tubes, crystallographic orientation in the sample does not allow easy twinning under tensile loading but twinning becomes favored under compressive loading. Accordingly, the {10–12} <10–11> twinning was activated under compressive stress but not in tensile stress along the extrusion directions of the tubes, which resulted in abrupt decrease of yield stress in compression and marked compressive-tensile asymmetric behavior. The occurrence of twinning was also clearly detected by metallographic observations. Consistently, the weaker texture found in the starting material resulted in lower evidence of asymmetry in mechanical properties and the AZ31 alloy that developed a slightly weaker texture after extrusion showed a less marked anisotropy.

Table 1 Tensile and compression 0.2 % offset yield strength of the as received bars and extruded tubes

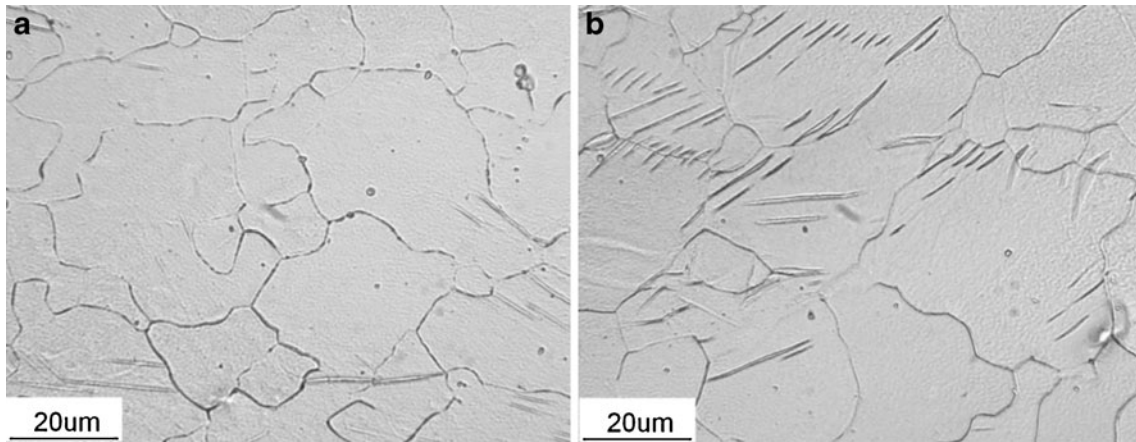|	ZM21			AZ31B	
	As received	Tube D6d3	Tube D8d6	As received	Tube D6d3
Compressive yield stress (MPa)	107.6	55.1	49.8	109.6	91.8
Tensile yield stress (MPa)	160.3	144.6	162.5	149.7	166.5
Loss of yield strength (compression vs. tension, in %)	32.9	61.9	69.4	26.8	44.9

Fig. 7 Microstructure of extruded ZM21 tubes after straining up to 2 %. **a** Tensile strained specimen; **b** compression strained specimen

Significance of anisotropy on performance of magnesium stents

The asymmetry observed in the mechanical behavior of hot-extruded magnesium alloy tubes may have a strong influence on the design and service response of magnesium stents. The deployment of the stents foresees the insertion into a human vessel of a catheter with an inflatable balloon where a stent is crimped, the stent expansion once reached the stenotic zone of the vessel and finally the scaffolding to the vessel (with some stent recoil). Usually, the stent structure is composed of two different types of elements (Fig. 8a): tubular-like rings composed by a sequence of U-shaped structures and bridging members (axial links). The former mainly act to sustain the vessel after the stent

expansion and the latter to link the rings in a flexible way, during the delivery process and once the stent is expanded. Accordingly, during expansion and scaffolding, the rings are mainly subjected to bending stresses. This behavior can be usefully verified performing finite element analyses (FEA) of the expansion of the stent into a vessel. In this work the results of the stenting procedure simulation described in [20] are reported. The studied stent, shown in Fig. 8a, resembles the existing Magic stent (Biotronic Inc., Germany) and it is composed of seven rings connected by straight links and presenting four peak-to-valley struts in the circular direction. It was reconstructed with an outer diameter of 1.4 mm, a longitudinal length of 8.0 mm, a thickness of 0.15 mm, a strut width of 0.08 mm [21]. The stent was assumed made by the magnesium alloy WE43, characterized by the
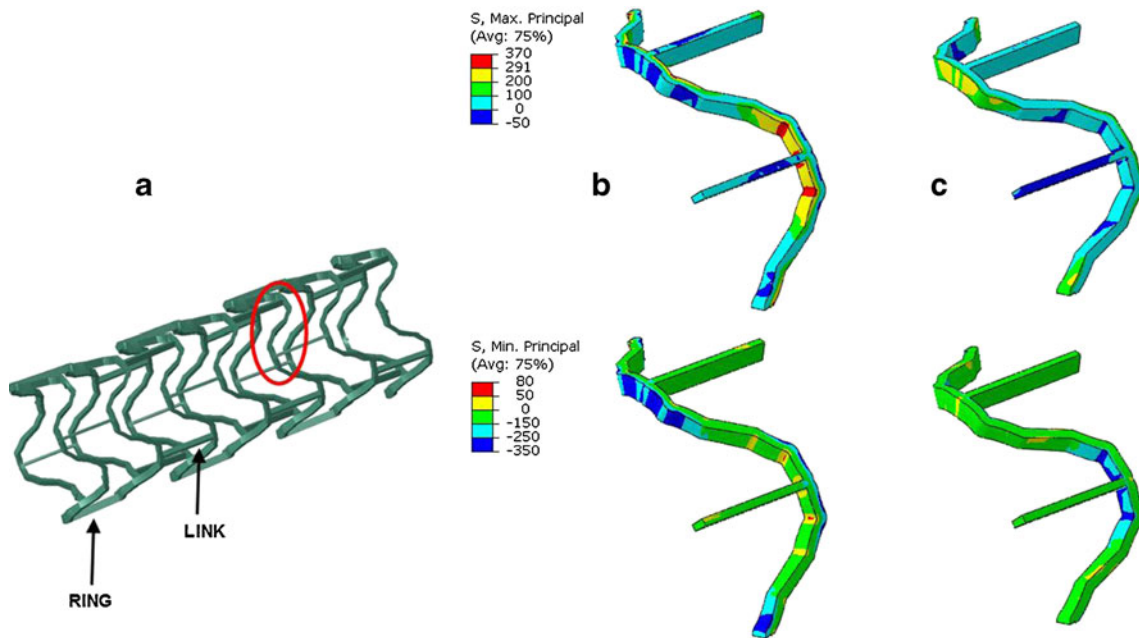

Fig. 8 General structure of a stent (**a**) and stress distribution of the stent net during the phase of expansion (**b**) and scaffolding (**c**)

following mechanical properties [22]: elastic modulus 45 GPa, Poisson's ration 0.3, yield stress 161 MPa, fracture elongation 0.183, density 1.74 g/mm3. The stent was meshed with solid elements. For simulating the expansion of the stent into a stenotic vessel a 3D model composed by the stent, a folded balloon and a vessel including the presence of a plaque were built and a quasi-static procedure of a FEA explicit solver was applied. For a detailed description of the whole finite element model (geometry, material, mesh, boundary and loading conditions) see [20]. In Fig. 8b and c the results of the simulations in terms of stress distribution into the U-shaped structures are reported: the maximum values at the intrados at the end of the expansion and maximum values at the extrados at the end of the scaffolding show that bending is prevelaing in the rings. These loading modes result in external tension and internal compression during scaffolding, and vice versa during expansion. Finite element method studies also revealed that inhomogeneous deformation of the metallic net and within the U-shaped structure induces a strong residual stress field in the material [23]. During the delivery and service in the stenotic vessel, the whole stent is bent and the links are again subjected to tension and compression depending on their position with respect to neutral axis [24]. The resulting extent of the residual and applied stress fields strongly affect fatigue performance [20] and stress corrosion cracking (SCC) behaviour, as already observed during slow strain rate testing (SSRT) in modified simulated body fluid [25].

The described crystal texture condition of the extruded tubes features the basal planes of the hcp lattice cells mostly aligned along the longitudinal section while the expected loading modes show compressive and tensile stress permanently applied normally to this plane, hence normal to the basal plane during stent expansion and crimping. Since the tensile yield strength of the material is predicted to be much higher than the compressive yield strength, the volume of material at the extrados of the U-shaped structure will suffer easier deformation during expansion and a redistribution of stress state due to asymmetric behavior will occur with respect to expected models derived from symmetrical material behavior.

The lack of consideration of the tensile-compression asymmetry effects of the material would therefore induce wrong evaluation of the strength of the stents, their fatigue and corrosion resistance. For a better understanding of these phenomena, detailed constitutive models of material behavior should be developed, taking into account of the tension-compression asymmetric behavior of Mg alloys after plastic deformation.

Conclusions

AZ31B and ZM21 magnesium alloys were extruded by a laboratory equipment at die temperature of 410 °C and strain rate of $2.78 \cdot 10^{-3} \, s^{-1}$ for the production of small size tubes to be used as precursors for biodegradable stent application. The experimental data collected suggested relationships between microstructure, texture and mechanical behavior and supplied information on stent design and modeling as summarized in the following points.

Recrystallization during the hot extrusion process allowed to form relatively fine and homogeneous microstructures in both alloys. Both starting alloys had a weak texture which evolved into a basal type texture, featuring the (0001) basal plane aligned parallel to the longitudinal section of the tubes.

An asymmetric material behavior was measured by tension and compression testing of the tubes, with a sharp decrease of yield strength in compression. This behavior was related to a preferred activation of the {10–12} <10–11> twinning system under compression straining.

The different deformation mechanisms activated in tension and compression were also confirmed by metallographic analyses. Compression tested specimens always featured a significant amount of twins in their structure. The AZ31B alloy developed a weaker texture and accordingly showed a less marked asymmetric behavior.

The asymmetric deformation behavior of the extruded magnesium alloys was considered in relation to service of stents, especially considering the stages of expansion and scaffolding. The importance of considering the above effects in stent design and modeling is highlighted in order to improve performance and reliability of such devices.

References

1. Stanford N, Sotoudeh K, Bate PS (2011) Deformation mechanisms and plastic anisotropy in magnesium alloy AZ31. Acta Mater 59:4866–4874
2. Pèrez-Prado MT, Ruano OA (2003) Texture evolution during grain growth in annealed Mg AZ61 alloy. Scripta Mater 48:59–64
3. Liang SJ, Liu ZY, Wang ED (2008) Microstructure and mechanical properties of Mg-Al–Zn alloy deformed by cold extrusion. Mater Lett 62:3051–3054
4. Kleiner S, Uggowitzer PJ (2004) Mechanical anisotropy of extruded Mg–6 % Al–1 % Zn alloy. Mater Sci Eng, A 379:258–263
5. Ball EA, Prangnell PB (1994) Tensile-compressive yield asymmetries in high strength wrought magnesium alloys. Scripta Metal 31(2):111–116
6. Erbel R, Di Mario C, Bartunek J, Bonnier J, De Bruyne B, Eberli FR, Erne P, Haude M (2007) Temporary scaffolding of coronary arteries with bioabsorbable magnesium stents: a prospective, non-randomized multicentre trial. Lan 369:1869–1875
7. Ron Waksman X, Erbel R, Di Mario C (2009) Early- and long-lerm intravascular ultrasound and angiographic findings after

bioabsorbable magnesium stent implantation in human coronary arteries. Card Inter 2:312–320

8. Wang WQ, Liang DK, Yang DZ, Qi M (2006) Analysis of the transient expansion behavior and design optimization of coronary stents by finite element method. J Biomech 39:21–32

9. Timmins LH, Moreno MR, Meyer CA, Criscione JC, Rachev A, Moore JE (2007) Stented artery biomechanics and device design optimization. Med Biol Eng Comput 45:505–513

10. Li N, Zhang HW, Ouyang HJ (2009) Shape optimization of coronary artery stent based on a parametric model. Fin Elem Ana Des 45:468–475

11. Martin D, Boyle FJ (2011) Computational structural modelling of coronary stent deployment: a review. Comput Meth Biomec Biomed Eng 14:331–348

12. Pant S, Limbert G, Curzen NP, Bressloff NW (2011) Multiobjective design optimisation of coronary stents. Biomater 32:7755–7773

13. Ge Q, Vedani M, Vimercati G (2012) Extrusion of magnesium tubes for biodegradable stent precursors. Mater Manu Pro 27:1–7

14. Agnew SR, Duygulu O (2005) Plastic anisotropy and the role of non-basal slip in magnesium alloy AZ31B. Inter J Plas 2:1161–1193

15. Huang S, Zhang S, Li D, Peng Y (2011) Simulation of texture evolution during plastic deformation of FCC, BCC and HCP structured crystals with crystal plasticity based finite element method. Trans Nonferr Met Soc China 21:1817–1825

16. Yi SB, Zaefferera S, Brokmeier HG (2006) Mechanical behaviour and microstructural evolution of magnesium alloy AZ31 in tension at different temperatures. Mater Sci Eng, A 424:275–281

17. Meyers MA, Vöhringer O, Lubarda VA (2001) The onset of twinning in metals: a constitutive description. Acta Mater 49:4025–4039

18. Li B, Ma E (2009) Zonal dislocations mediating{10–11} <10-1-2> twinning in magnesium. Acta Mater 57:1734–1743

19. Wang YN, Huang JC (2007) The role of twinning and untwining in yield behavior in hot-extruded Mg-Al-Zn alloy. Acta Mater 55:897–905

20. Wu W, Petrini L, Gastaldi D, Villa T, Vedani M, Lesma E, Previtali B, Migliavacca F (2010) Finite element shape optimization for biodegradable magnesium alloy stents. Ann Biomed Eng 38:2829–2840

21. Erbel R, Di Mario C, Bartunek J, Bonnier J, de Bruyne B, Eberli FR, Erne P, Haude M, Heublein B, Horrigan M, Ilsley C, Bose D, Koolen J, Luscher TF, Weissman N, Waksman R, Investigators P-A (2007) Temporary scaffolding of coronary arteries with bioabsorbable magnesium stents: a prospective, non-randomised multicentre trial. Lancet 369:1869–1875

22. Muller H (2009) Development of metallic bioabsorbable intravascular implants. New Tech Vasc Biomat 23–32

23. Lin H, Hsu Y, Keh C (2008) Inhomogeneous deformation and residual stress in skin-pass axisymmetric drawing. J Mater Proc Tec 201:128–132

24. Gastaldi D, Sassi V, Petrini L, Vedani M, Trasatti S, Migliavacca F (2011) Continuum damage model for bioresorbable magnesium alloy devices application to coronary stents. J Mech Beh Biomed Mater 4:352–365

25. Choudhary L, Szmerling J, Goldwasser R, Raman RKS (2011) Investigations into stress corrosion cracking behaviour of AZ91D magnesium alloy in physiological environment. Proc Eng 10:518–523